

Efficient Multi-walled Carbon Nanotubes/Iron Oxide Nanocomposite for the Removal of the Drug Ketoprofen for Wastewater Treatment Applications

Ismail Badran*^[a] and Maan Omar Al-Ejli^[b]

Current environmental restrictions, such as the zero liquid discharge policy, require developing new methods to completely remove micropollutants from wastewater. Non-steroidal anti-inflammatory drugs (NSAID) are major component of such pollutants. The adsorptive removal of ketoprofen (KP), a widely prescribed NSAID, was studied using a newly synthesized magnetic adsorbent. The maximum adsorption capacity was determined to be 39.2 mg/g with almost 98% removal for 50 mg/L KP at neutral pH. The adsorption of KP was found to be pH dependent and more efficient in acidic media. The

isothermal behavior of the adsorbent followed a sigmoidal behavior and was best fitted to the corresponding-states equation (CSE). The adsorption was found to follow second-order kinetics with a half-life of 4.4 min. The adsorption was also found to be exothermic and therefore it is favorable at low temperatures. The study also showed that the adsorbent can be regenerated for several adsorption-desorption cycles. The adsorption mechanism was also explored by state-of-the-art periodic quantum theoretical calculations.

Introduction

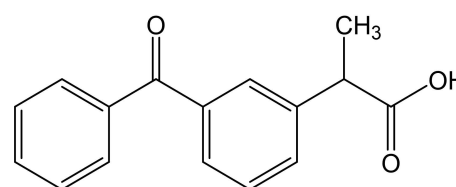
The global increase in urbanization, industrialization, and consumption is posing a huge demand for freshwater resources.^[1–3] Water contamination and overuse of water resources are two of today's significant issues.^[4–5] New policies, such as the zero liquid discharge (ZLD) and minimal liquid discharge (MLD) frameworks, are currently in place to address such challenges.^[6–8] The ZLD and MLD policies aim to maximize water recycling and limit wastewater discharge to the environment.

Over the course of last years, a new class of emergent pollutants have entered the water system due to industrial expansion and use. Such pollutants include pharmaceutical and personal care products (PPCP).^[9–11] PPCP were proven to pose risks to human, animal, and aquatic life if incorrectly administered or existed in water resources above certain limits.^[1,12–13] Traditionally, several wastewater techniques such as coagulation and flocculation, centrifugation, advanced oxidation, aerobic and anaerobic treatments are employed. But because PPCP cannot be eliminated using conventional approaches, new technologies are required to satisfy the ZLD and MLD standards.^[3,14–16]

Advances in nanotechnology have led to the development of several types of materials that can remove pollutants from contaminated water with high efficiency.^[11,17] 2D carbon-based nanomaterials, such as graphene and carbon nanotubes, are among the most robust and efficient in this field, due to their exceptional properties in molecular separation and transport.^[18]

Non-steroidal anti-inflammatory drugs (NSAID) are considered a new class of emerging pollutants that harms our environment.^[19–21] The problem of NSAID is two folds: first, their complex structure and reactivity that can pose risks on human as well as aquatic life.^[9,22–23] Second, they are created in enormous quantities and can accumulate in water resources due to their persistence. In fact, NSAID have been detected in municipal and natural water systems across the globe.^[15,24–26] Although there is no solid evidence on the toxicity of NSAID to adults, they may very well be toxic to aquatic organisms, embryos, infants, and vulnerable species.^[19] In fact, the adverse effects of NSAID and pharmaceuticals are not very well understood due to their long side effects.^[22,26] Such adverse effects might involve cancer, infertility, allergy, antibiotic resistance, and endocrine disorders.^[19,26]

Ketoprofen (KP), shown in Scheme 1, is an NSAID that was approved for medical use for the first time in 1980.^[27] The drug is commonly prescribed to treat a wide range of acute and chronic inflammation conditions including, muscle aches, nerve



Scheme 1. Molecular structure of ketoprofen.

[a] Dr. I. Badran

Department of Chemistry
Faculty of Sciences, An-Najah National University
Nablus, Palestine, P.O.Box: 7
E-mail: i.badran@najah.edu

[b] M. O. Al-Ejli

Department of Chemistry and Earth Sciences

College of Arts and Sciences, Qatar University
P.O. Box: 2713, Doha, Qatar College of Arts and Sciences, Qatar University



Supporting information for this article is available on the WWW under <https://doi.org/10.1002/slct.202202976>

pain, and osteoarthritis.^[20,28–29] Despite its wide usefulness, KP is found to have some adverse digestive problems such as diarrhea, bloating, and constipation.^[20] Recently, the U.S. Food and Drug Administration (FDA) required all ketoprofen packages to be labeled to describe the risk of kidney problems in unborn babies. The drug is not currently recommended for pregnant women after their 20 weeks of pregnancy.^[30] KP is also found to be very toxic to bacteria and some other microorganisms, which are not necessarily harmful themselves.^[26] Using KP in veterinary medicine also led to a detrimental impact on vulture populations and the mortality of male eider ducks.^[31] With these considerations in mind, KP was chosen as a model NSAID water contaminant in this study.

This work is also motivated by the detection of KP in several water resources across the globe.^[19,32–34] For instance, the drug was detected in amounts ranging from 0.2–3.5 mg/L in effluent water samples in France and other parts of Europe.^[35–36] In South Africa, KP, along with aspirin, was the most abundant drug detected in surface water. Thus, we decided to develop a method to remove KP, and possibly other NSAID, from aqueous media for future wastewater treatment technology development.

In our quest to develop an efficient adsorbent to remove ketoprofen, we aimed for a material that is stable, non-toxic, economical, and easily produced and recycled at industrial scales. Iron oxides are novel adsorbents that match these criteria; they can also be functionalized to target certain pollutants.^[37–42] Therefore, we chose magnetite (Fe_3O_4) as the main adsorbent in this study due to its stability and facile preparation. Although magnetite is cheap and abundant in the earth's crust, it suffers low adsorption capacity compared to some other novel adsorbents. Thus, we used multi-walled carbon nanotubes (MWCNT) to produce a highly stable nanocomposite of Fe_3O_4 /MWCNT (referred herein by Fe/CNT). The CNT serves as an excellent adsorbent due to their high surface area, in addition to their high thermal and chemical stability.^[43–47] By this, the nanocomposite will combine the benefits of highly efficient CNT with the low cost of Fe_3O_4 and thus can be produced on a high scale.

Several studies have been published on the adsorptive removal of KP from aqueous solutions utilizing various natural and synthetic materials. Kerkhoff et al. have used activated carbon (AC) for the removal of KP and they reported a good adsorption capacity of 108.08 mg/g but the removal efficiency was not complete (~85%), and the adsorption was fairly slow.^[48] Rizzi et al. used natural chitosan solid films and achieved 90% removal efficiency.^[49] Madikizela et al. have developed molecularly imprinted polymer (MIP) to remove KP from water, but they reported a fairly low adsorption capacity of 8.2 mg/g.^[50] In addition, Lawal et al. have combined carbon nanotubes with ionic liquid and achieved a very high adsorption capacity of 410 mg/g, but the adsorption was too slow with a reported equilibrium time of 24 hours.^[51] Although these materials (AC, CNT, MIP and chitosan) have demonstrated good performance in adsorption KP, none of them demonstrate magnetic properties that allows them to be easily separated at the end of the adsorption process. Recently, few

efforts have been made to fabricate magnetic materials capable to remove KP from aqueous medium, including NiFe_2O_4 /AC,^[32] Bi_2MoO_6 ,^[52] and MnFe_2O_4 .^[53] In these works, the removal efficiency ranged between 70–85%, indicating that complete removal was never achieved. In this work, we target a complete solution for this problem by fabricating an Fe/CNT nanocomposite combines the benefits of the excellent adsorption capacity of MWCNT, and the ferrimagnetic nature of iron oxide that facilitates their separation and reuse in real applications. As we show herein, the adsorbent demonstrated excellent performance with almost complete removal of the drug. More importantly, this work aims to comprehend the adsorption of KP on the adsorbent surface by taking advantage of modern computational techniques.

In order to optimize the conditions for the adsorptive removal of KP, the effects of adsorbent dosage, solution pH, shaking time, and temperature were examined. Also, the adsorption kinetics were studied by following the adsorption equilibrium of KP over time. Finally, a regeneration study was done in an attempt to reuse the adsorbent. To better understand the adsorption mechanism, the interactions of the drug with either Fe_3O_4 and CNT was explored by periodic DFT calculations. The results of this work were compared to previous studies on KP removal to outline the advantages of the method used in this work.

Results and Discussion

Fe_3O_4 /MWCNT Adsorbent characterization

The aim of this work was to synthesize a highly magnetic nano-adsorbent that can be easily separated from the bulk solution. Figure 1 demonstrates how easy it is to separate the newly synthesized Fe/CNT nanocomposite using a neodymium magnet. It is noteworthy to mention that the aqueous media was tested by UV-Vis spectrophotometry after the separation of the solid, and no contamination was observed. The prepared Fe/CNT nanocomposite was then characterized by scanning electron microscopy. The SEM image for the pure MWCNT (magnified x50,000) is shown in Figure 2-a. The MWCNT were

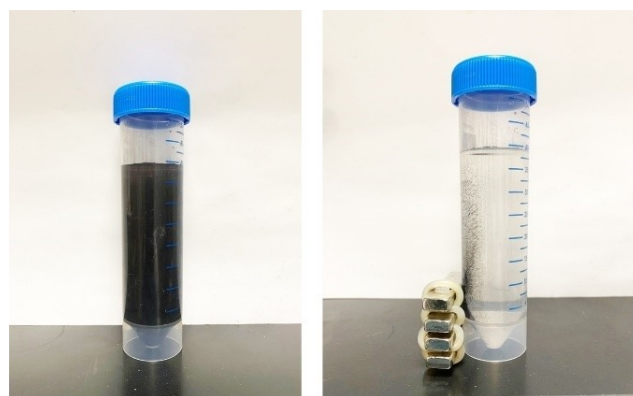


Figure 1. Separating the Fe/CNT nanocomposite by a neodymium magnet.

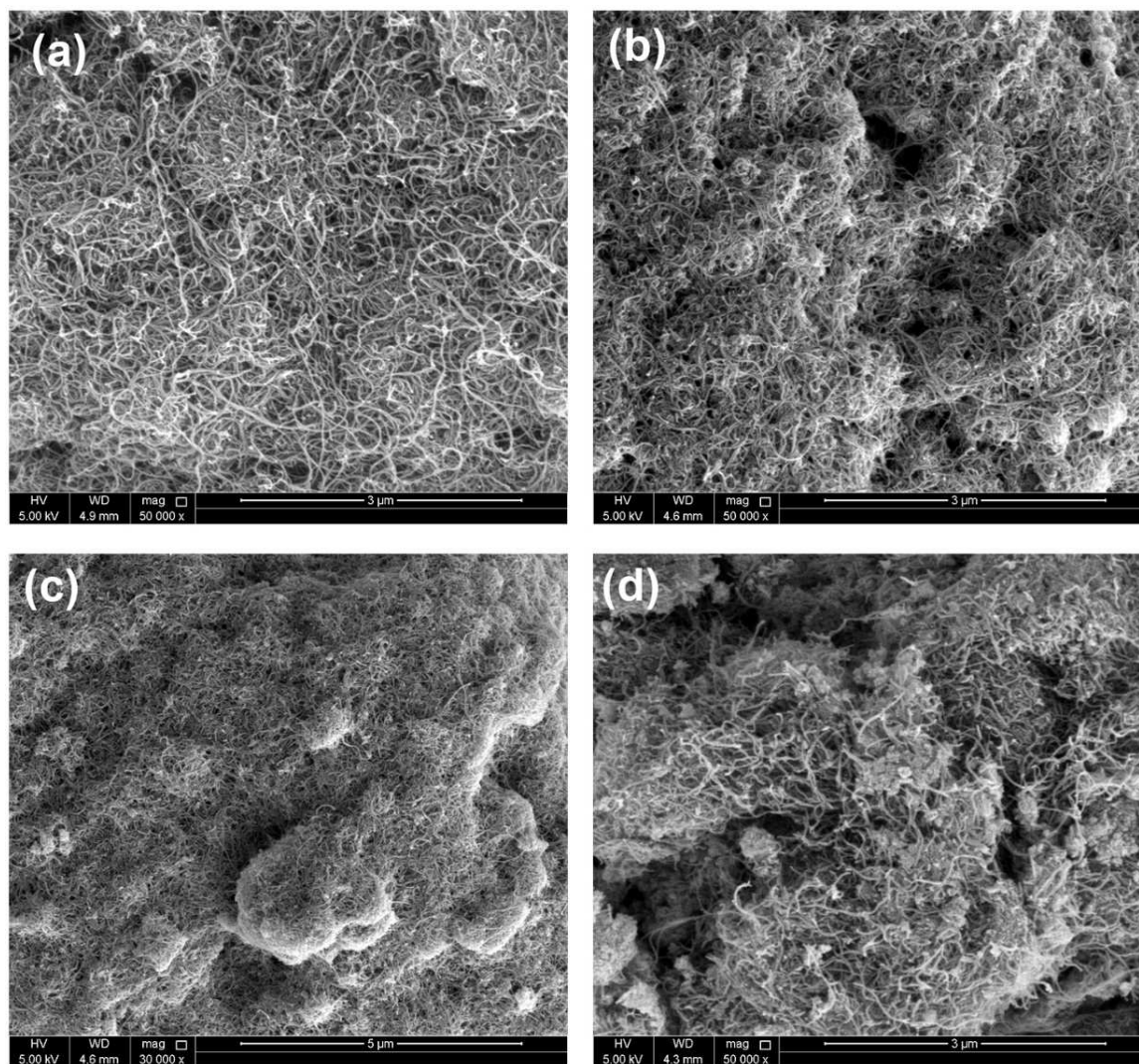


Figure 2. Scanning electron microscope (SEM) images for a) native MWCNT, b) Fe/CNT, c) Fe/CNT (zoom out), and d) Fe/CNT after adsorption with ketoprofen.

determined to be ~ 10 – 20 nm in width and 100 nm to a few μm in length, in agreement with our last work.^[43] Upon the treatment with maghemite, the Fe/CNT formed a 'spongy' structure as seen in Figure 2-b. This indicates an increase in the crosslinking between the CNT and the iron oxide crystals. The EDX data (supporting information section, Figure S3-S5) obtained from the samples in Figure 2-b indicated a CNT percentage of about 25%. Figure 2-c and -d show the SEM images for the nanocomposite after one adsorption test with ketoprofen. The presence of the drug is not highly visible from the images, neither from the EDX data. This is due to the fact that MWCNT operates by adsorbing organic molecules on the outside surface as well as inside the tubes.^[43,54–55] Nevertheless, few accumulations of solid can be viewed in Figure 2-d as white spots, which represent the adsorbed drug's deposits.

Figure 3-a shows the X-ray powder diffraction (XRD) patterns for the Fe/CNT nanocomposite along with its pure precursors. The XRD diffraction pattern for Fe_3O_4 agrees very well with its recorded miller indices at 202, 311, 400, 242, 511,

and 404. After treatment with CNT, the XRD pattern and the degree of crushability of the iron oxide were not affected as seen from the figure. The spectrum also shows the absence of any impurities in the sample. Although the CNT exhibits a broad diffraction peak at around 15° , this peak is not visible in the Fe/CNT spectrum. This is mostly due to the crosslinking between the CNT and the Fe_3O_4 lattice structure.

Figure 3-b shows the FTIR spectrum for the synthesized Fe/CNT. The spectrum shows a peak at 535 cm^{-1} that is characteristic of Fe–O bond stretching in Fe_3O_4 .^[54] The band at 1110 cm^{-1} is assigned to C–O bond stretching in alcohols or carboxylic acids. The fact there is a peak at 1630 cm^{-1} corresponding to carbonyl (C=O) group suggests the presence of carboxylic acid groups on the CNT surface, as commonly known in commercial MWCNT samples.^[54,56] The FTIR peak at 1580 cm^{-1} is assigned to C–C bond stretching in the CNT structure, while the one at 3350 cm^{-1} (–OH) is mostly due to the presence of some water in the sample.

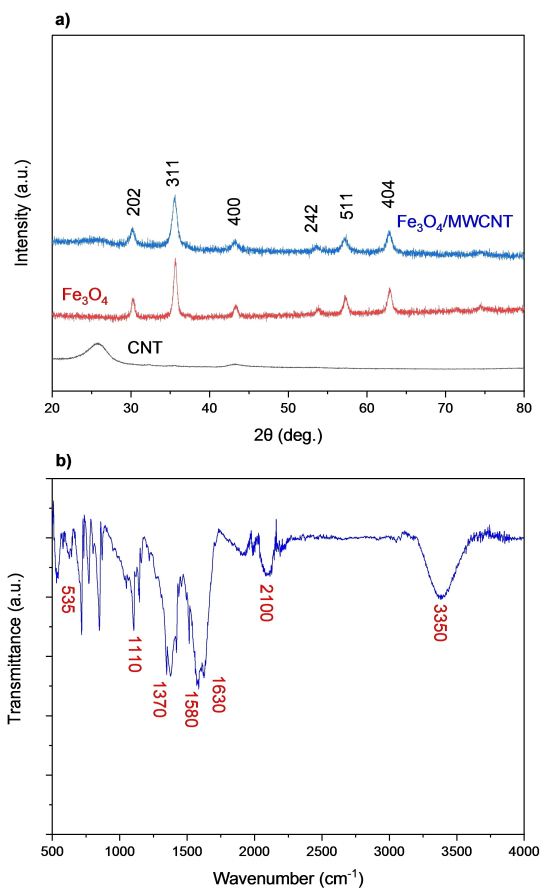


Figure 3. a) X-ray powder diffraction patterns for pure MWCNT, Fe_3O_4 , and the $\text{Fe}_3\text{O}_4/\text{MWCNT}$. b) FTIR spectrum of $\text{Fe}_3\text{O}_4/\text{MWCNT}$ composite.

Adsorption of ketoprofen by Fe/CNT nanocomposite

To investigate the adsorptive removal of KP, the drug's UV-Vis absorbance spectrum was recorded, and it exhibits strong absorbance in the UV region with $\lambda_{\text{max}} = 260$ nm, as seen in Figure S6. A calibration curve was constructed using standard solutions of KP in deionized water as illustrated in Figure 4. The

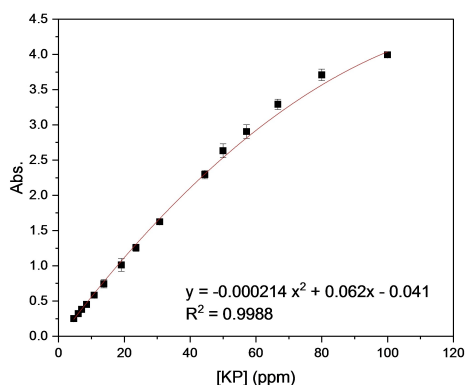


Figure 4. Calibration curve for ketoprofen standard solutions at 25°C , and $\text{pH} \approx 7$.

error bars in the curve represent the standard deviation of three trials. The curve followed a quadratic equation with an R^2 of 0.9988. Thus, this fitting was used to determine the KP concentration for the rest of this work. The effect of shaking time on the adsorption of KP was studied for up to 60 min and it is depicted in Figure 5. This part of the study was done using a fixed concentration KP and Fe/CNT adsorbent. As illustrated, the adsorption removal of KP reaches its maximum after 20 min. Therefore, this value was selected for the rest of this work. More information on the reproducibility, selectivity, the detection limit, and sensitivity of the method used in this work can be found in the supporting information section.

The adsorption isotherms for KP were studied by varying the amount of adsorbent at room temperature and using a fixed concentration of 50 mg/L of the drug. The adsorption was highly efficient as illustrated in Figure 6-a. The maximum removal efficiency obtained in this work was 98.3%. This is higher than what was obtained for the adsorption of KP using copper nanoparticles (89%)^[20] or porous carbon (92%)^[19]. This is because of the dual nature of the nano adsorbent and the high adsorption capacity of CNT employed in the present work.

Three isotherms at different pH values (6.3, 7.7, and 9.5) were constructed and shown in Figure 6-b. The effect of pH on the adsorption of KP will be discussed in the next section. Interestingly, the adsorption isotherms followed a sigmoidal behavior as seen in Figure 6-b. It is widely agreed that an S-shaped isotherm is observed when competition between monolayer and multilayer coverage exists.^[57–58] In the middle section of the isotherm, which is almost linear as in the case of Figure 6-b, the monolayer coverage comes into completion and multilayer adsorption starts. In other words, an S-shaped isotherm is mostly regarded as a result of at least two opposite adsorption mechanisms.^[59]

In our attempt to fit the adsorption data into an S-shaped adsorption model, we fitted the results into the corresponding-states equation (CSE) suggested by Radke and Prausnitz.^[60]

$$q_e = q_m [1 + k_1 C_e + k_2 C_e^2 + k_3 C_e^3] \quad (1)$$

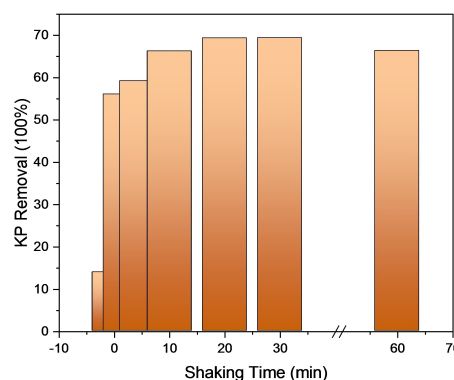


Figure 5. Effect of shaking time on the adsorption of ketoprofen at 25°C , and $\text{pH} \approx 7$. [KP] = 50 mg/L, solution volume = 25 mL, amount of adsorbent = 50 mg.

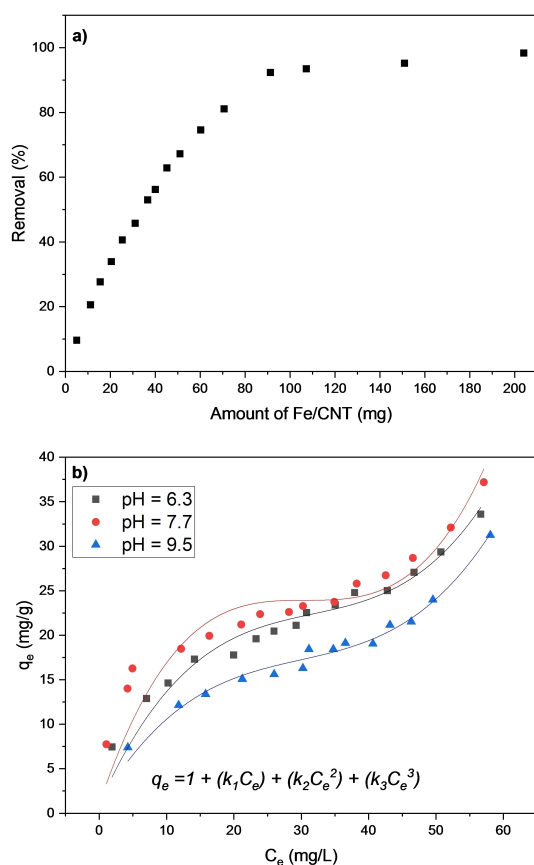


Figure 6. a) The adsorptive removal of KP (50 mg/L) using different amounts of Fe/CNT at pH = 7.5. b) Adsorption isotherms of KP onto Fe/CNT with non-linear fitting curves according to the CSE model at different pH values. Shaking time = 25 min, shaking speed = 350 rpm, T = 25 °C.

where the constants (k_i) are called the adsorption virial coefficients, C_e is the adsorbate concentration at equilibrium, and q_e is the adsorption capacity at equilibrium and is defined by:

$$q_e = \frac{C_0 - C_e}{W} V \quad (2)$$

Applying eq. 1 gives a type-V isotherm for $k_0 > 0$, $k_1 < 0$ and $k_2 > 0$. The fitting results for this model are listed at the end of Table 1. The signs of k_i are in agreement with the aforementioned fact, and the regression coefficient R^2 was 0.9847. This infers that the CSE model managed successfully to describe the KP adsorption on the Fe/CNT surface. This is also in agreement with the dual mechanism theory, where the adsorption switches from monolayer coverage on the Fe_3O_4 surface, into multilayer adsorption on the surface of the carbon nanotubes.^[57]

In addition to the CSE model, we also tried the sigmoidal Langmuir model, as shown in Table 1. A poor fitting was obtained with an R^2 value of 0.5937. We also fitted the data to other models including BET, Langmuir, Freundlich, and Sips. The fitting graphs are shown in supporting information section

Table 1. Fitting parameters for the batch adsorption of KP.

Adsorption models fitting	
BET	
Model	$q_e = \frac{q_m K C_e}{(C_e - C)(1 + (K-1)(\frac{C_e}{C}))}$
q_m	1.8
K	28.5
C	1.6
Adj. R^2	0.8585
Langmuir	
Model	$q_e = \frac{q_m K_L C_e}{1 + K_L C_e}$
q_m	39.2
K_L	0.1
Adj. R^2	0.8161
Freundlich	
Model	$q_e = K_F C_e^{\frac{1}{n_F}}$
K_F	4.94
n_F	2.25
Adj. R^2	0.9135
Sips	
Model	$q_e = \frac{q_m K_S C_e^{\frac{1}{n_S}}}{1 + K_S C_e^{\frac{1}{n_S}}}$
q_m	2.9×10^6
K_S	1.8×10^{-6}
n_S	2.25
Adj. R^2	0.9059
Sigmoidal Langmuir	
Model	$q_e = \frac{q_m K_L C_e}{1 + K_L C_e + \frac{C_e^2}{S}}$
q_m	26.08
K_L	2.2×10^{44}
S	4.0×10^{45}
Adj. R^2	0.5937
CSE	
Model	$q_e = q_m [1 + k_1 C_e + k_2 C_e^2 + k_3 C_e^3]$
q_m	6.19
k_1	0.19
k_2	-5.24×10^{-3}
k_3	6.03×10^{-5}
Adj. R^2	0.9847

(Figure S7). The fitting results along with the fitting parameters are all listed in Table 1. It is noteworthy to mention that Freundlich fitting ($R^2 = 0.9135$) was better than that of the Langmuir model ($R^2 = 0.8161$). This supports the notion that the adsorption is indeed a multilayer one.

A closer look at Figure 6 indicates that the maximum adsorption capacity (q_m) of the Fe/CNT adsorbent in our experiments was between 30–40 mg/g. It is common to determine the exact value of q_m from a Langmuir fitting. In our case, this value is averaged at 39.2 mg/g for the three pH isotherms. This value is lower than the one obtained in our recent work where CNT was used in a fixed-bed column, where $q_m = 275.3$ mg/g.^[43] It is also higher than the one we obtained using Fe_2O_3 nanoparticles where $q_m = 23.2$ mg/g,^[39] or activated carbon (7.6 mg/g).^[61] More correlations with previous studies on KP are to be discussed at the of this paper.

Effect of solution pH

It is known that sorption capacity can be affected by the solution's pH through the electrostatic attractions or repulsions within the adsorbent/adsorbate sphere.^[37,43] In addition, the sorption mechanism can be affected by changes in the polarity of the functional groups as pH changes. The effect of solution pH on the adsorptive removal of KP into the Fe/CNT nanocomposite was studied in the range of 3–11. This part of the study was performed by preparing buffered solutions with different pH values as described in the experimental section. Figure 7-a shows the dependence of the KP removal on the solution pH. As the pH increases, the removal efficiency decreases. The best removal was obtained at pH=4.7. In order to explain this finding, the point of zero charge (PZC) of the Fe/CNT adsorbent was determined as explained in the experimental section. Figure 7-b shows that the PZC, represented by the cross point between the initial and final pH, is equal to 5.7. This means that the Fe/CNT adsorbent would have a net positive charge below pH=5.7, and a net negative charge above that value. Meanwhile, the reported pKa value for the KP drug is 4.45.^[20] This infers that the drug exists in its protonated form under pH=4.45, and in its anionic form above that value. Given these facts, it is expected that the KP bonds strongly with the MWCNT surface in the lower pH region. This is achieved by

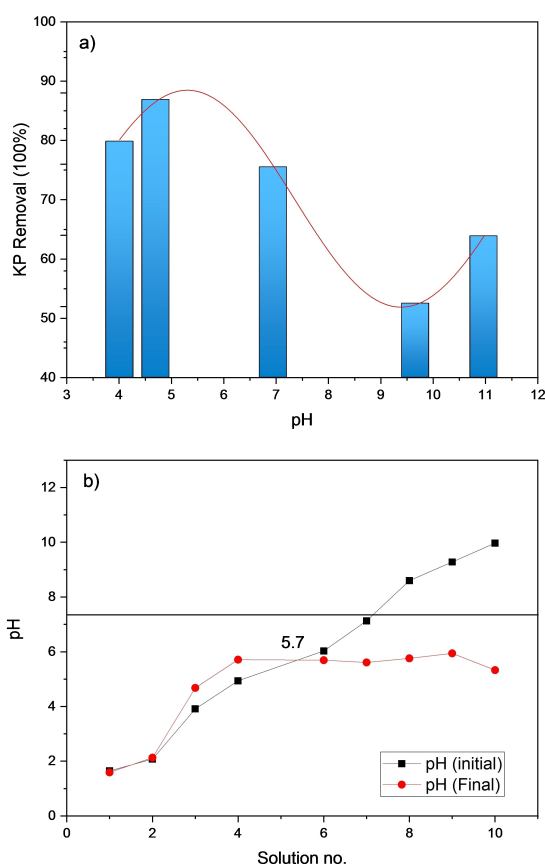


Figure 7. a) effect of solution pH on the adsorption of 50 mg/L KP onto 100 mg of Fe/CNT. Amount of adsorbent = 100 mg, solution volume = 25 mL, T = 25 °C. b) determining the point of zero charge for the Fe/CNT adsorbent.

electrostatic interactions and H-bonding between the carboxylic group in the drug (*cf.* Scheme 1) from one side, and the polar functional groups on the CNT surface or the oxygen acidic sites in Fe₃O₄.^[20,39, 54] At higher pH values, the drug transforms into its anionic form, and repulsion forces with the negatively charged surface can hinder the adsorption process, leading to a notable decrease in the adsorption efficiency. This observation agrees well with previous studies that utilized MWCNT as an adsorbent,^[20,22,62–64] including our recent work on glimepiride.^[43]

Effect of contact time, adsorption kinetics

The adsorption kinetics of KP on the Fe/CNT surface was studied by following the concentration of the drug in aqueous media over time. A plot of q_e vs. time is shown in Figure 8. The data were fitted to different adsorption kinetics models. The pseudo first-order model (PFO) is given by:^[65–66]

$$q_t = q_e(1 - e^{-k_1 t}) \quad (13)$$

and the pseudo second-order (PSO) model is defined by:

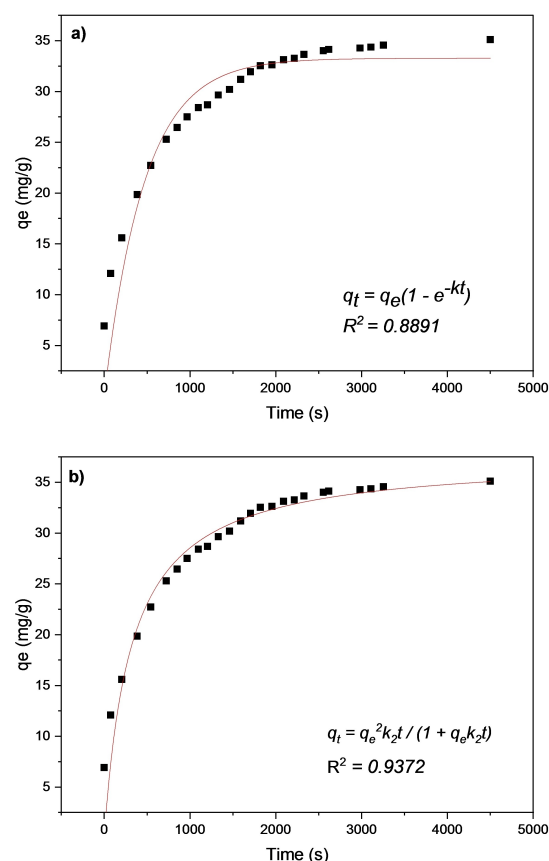


Figure 8. The change of the equilibrium adsorbate concentration (q_e) of KP over time. a) nonlinear fitting for pseudo first-order, and b) second-order kinetics. KP concentration 45.0 mg/L, amount of adsorbent = 15 mg, shaking speed 350 rpm, solution pH \approx 7. T = 25 °C.

$$q_t = \frac{q_e k_2 t}{1 + q_e k_2 t} \quad (4) \quad \ln K = \frac{-\Delta H^\circ}{RT} + \frac{\Delta S^\circ}{R} \quad (7)$$

where q_e and q_t (mg/g) are the adsorption capacities at equilibrium and time t , respectively, and k_1 and k_2 are the rate constants for the pseudo first- and second order models, respectively. Nonlinear fittings for the two models are shown in Figure 8. The best fitting was obtained for the PSO model with a regression coefficient $R^2 = 0.9372$. We need here to emphasize that we attempted to fit other kinetic models, such as the Elovich, Ritchie, and the mixed order models, but the best fitting was still obtained for the PSO model. There is an enormous number of studies where the PSO model was best describing the adsorption kinetics as recently listed by Wang and Guo.^[66] In addition, the adsorption of KP itself was reported to follow second-order kinetics.^[20,22] At the molecular level, adsorption with a PSO kinetics suggests that the adsorbent is abundant with active sites.^[66] This agrees very well with the nature of the adsorbent synthesized in this work, as MWCNT are known to have a high surface area with plenty of internal and external active sites. It is noteworthy to mention that some studies on KP removal have reported first-order kinetics. This is because such studies have employed single adsorbents such as copper nanoparticles^[20] or porous carbon,^[19] which might have fewer active sites than the MWCNT used in this work.

Using the nonlinear fitting of Figure 8-b. the second-order rate constant for the adsorption of KP was determined to be $5.7 \times 10^{-3} \text{ min}^{-1} \text{ mg}^{-1} \text{ L}$. Thus, the half-time of adsorption is evaluated at 4.4 min. This is close to what was recently obtained by Ouasfi *et al.* (8.4 min).^[19] This also infers that the adsorptive removal of KP is relatively fast, where half its initial concentration is removed within less than 5 min.

Effect of temperature and thermodynamical analysis

In the previous sections, we described the effect of different environmental parameters on the adsorption of KP under isothermal conditions. In this section, we discuss the effect of changing the solution's temperature on the adsorption of KP, which helps to deduce the thermodynamic parameters needed to comprehend the adsorption mechanism.

The change in Gibbs free energy (ΔG) is related to the equilibrium constant through the Van't Hoff equation:^[67-68]

$$\Delta G^\circ = -RT \ln K \quad (5)$$

where R is the universal gas constant, and T is the temperature in K. The fundamentals of thermodynamics states that:

$$\Delta G^\circ = \Delta H^\circ - T\Delta S^\circ \quad (6)$$

where ΔH° and ΔS° are the changes in standard enthalpy and entropy, respectively. Eq's 5 and 6 rearrange to:

Thus, a plot of $\ln K$ vs. $1/T$ (in K^{-1}) should yield a linear relationship with a slope $= -\Delta H^\circ/R$ and an intercept $= \Delta S^\circ/R$.

According to a recent critical review by Lima *et al.*^[67] several works were reported to misuse these equations to obtain the thermal properties through applying a simplified Arrhenius plot that does contain the equilibrium constant K . For instance, by plotting the natural logarithm of concentration vs. $1/T$ from one single experiment. This was shown to introduce large errors in determining the thermal parameters. The authors stated that the correct way to evaluate the value of K for adsorption systems is to "obtain isotherms of adsorption at different temperatures and making the nonlinear fitting of the isotherms".^[67,69] Therefore, we have performed a series of adsorption experiments at four different temperatures in the range of 10–70 °C. At each temperature, an adsorption isotherm was constructed, and the results are shown in Figure S8. Next, each adsorption isotherm was fitted to the Langmuir adsorption isotherm (see Table 1) and K_L was determined as seen in Figure S7. Then, the values of K_L 's were used to construct the Arrhenius relationship according to eq. 7 and the plot is shown in Figure 9. An excellent regression coefficient value was obtained ($R^2 = 0.999$). As per eq's 6 and 7, the values of ΔH° and ΔS° are determined to be -38.0 kJ/mol and $-158.9 \text{ JK}^{-1} \text{ mol}^{-1}$, respectively. This infers that the adsorption of KP on the Fe/CNT surface is exothermic. The negative value of ΔS° implies a decrease in entropy as a result of accumulating the KP molecules on the surface, which is accompanied by a decrease in the translational entropy of the system. The exothermicity of this adsorption and the negative value of ΔS° are in concert with previous studies on MWCNT^[20,64,70] or using KP as an adsorbate.^[32]

Using eq. 6, the Gibbs free energy of adsorption (ΔG°) can be determined to be 9.4 kJ/mol . This value indicates that adsorption of KP on the Fe/CNT surface is chemical rather than physical. This is supported by the fact that adsorption isotherm

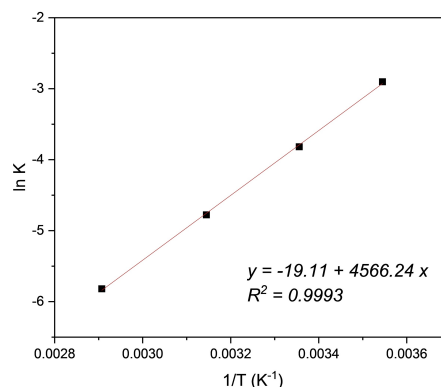


Figure 9. Arrhenius plot of $\ln K$ vs. $1/T$ to determine the thermodynamic parameters for the adsorption of KP into the Fe/CNT.

Table 2. Comparison between the results obtained in this work with previous studies.

Adsorbent	Adsorbent pore size (nm)	Adsorption capacity (mg/g)	Concentration range (ppm)	Optimum pH	Equilibrium time (min)	Removal efficiency (%)	Isotherm model	Ref.
3D graphene-based material + caffeic acid	–	125.4	10–80	6.6	720	–	Langmuir	[71]
Sonicated activated carbon	3–10	79.1	2–100	2.0	300	–	Sips	[72]
NiFe ₂ O ₄ /activated carbon magnetic composite	7.6	97.8	2–100	2.0	240	86.5%	Sips	[32]
Carbon nanotubes/ionic liquids	–	410.5	10–200	> 5.0	1440	> 80%	Freundlich	[73]
Activated carbon	1.2	108.8	0–300	6.7	120	84.8%	Freundlich and Langmuir	[48]
Molecularly imprinted polymer MIP	11.3	8.2	60–70	5.0	45	> 90%	Langmuir	[50]
Chitosan solid films	–	–	1.25–2.5	5.0	120	90%	–	[49]
Activated carbon	3.6	146.5	25–125	3.0	300	–	Double-layer model	[74]
Fe ₃ O ₄ -MWCNT	10–20	39.2	2–50	4.0	90	98%	Corresponding-states equation	This work

follows a sigmoidal behavior where the process switches from monolayer to multilayer coverage.

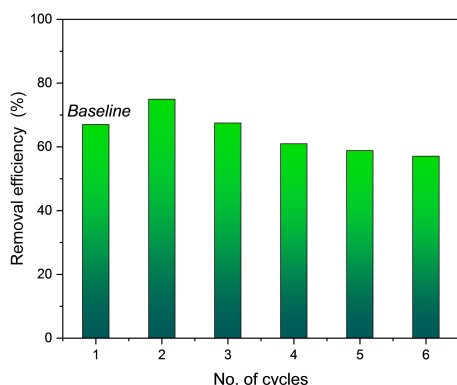


Figure 10. Reusability of the Fe/CNT NPs for adsorption/desorption of KP during six adsorption-desorption cycles using 0.1 M HNO₃. The initial concentration of KP = 55 mg/L, amount of adsorbent = 100 mg, pH = 4.01, shaking rate: 350 rpm, shaking-contact time: 10 mins, 25 °C.

Correlations with previous studies

In the previous sections, the adsorption of KP on the newly synthesized Fe/CNT composite showed an efficient, quick, and easy process to treat contaminated water from such pharmaceuticals. The adsorptive removal of the drug was investigated by several groups as shown in Table 2. Interestingly, the removal efficiency (98%) obtained in this study is the highest among all other previous studies. Also, the adsorption kinetic demonstrate a quick adsorption that reaches equilibrium within 90 min. Previous experiments on KP adsorption reported equilibrium times that exceed this number as shown in Table 2, except that reported by Madikizela et al. (45 min) where molecularly imprinted polymer (MIP) was used. Although the adsorption capacity obtained in this work (39.2 mg/g) was not much higher than previous studies, the advantage of the method described herein lies in synthesizing a magnetic adsorbent that can be easily separated from the bulk solution. Adsorbents such as activated carbon or pure CNT might provide higher adsorption capacities as shown in Table 2, but such adsorbents would be more expensive and not easily separable as the Fe/CNT.

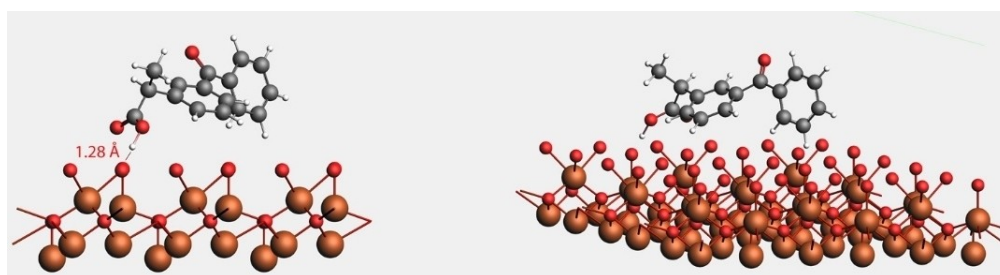


Figure 11. Optimized geometry of KP adsorption on Fe₃O₄ surface, obtained at PBE-D/DZP level of theory.

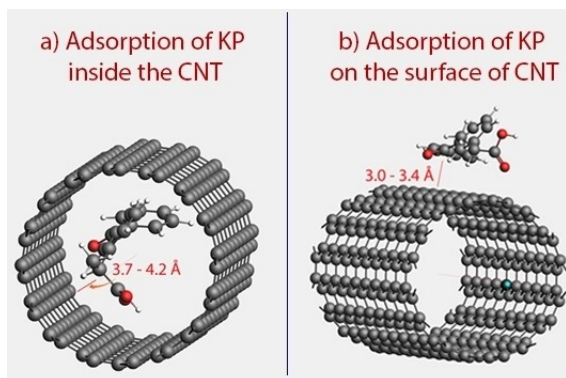


Figure 12. Optimized geometry of KP adsorption a) inside the CNT, and b) on the surface of CNT, obtained at PBE-D/DZP level of theory.

Regeneration of adsorbent

The results obtained in the previous sections point to a promising method for removing NSAID, such as KP, from contaminated water. In order to bring this method to practice and be environmentally friendly, we analyzed the regeneration of the adsorbent by chemical etching. First, we attempted to regenerate the adsorbent by washing the solid residue left after adsorption by 1.0 M HNO_3 and 1.0 M NaOH . We found that HNO_3 was more efficient in regenerating the Fe/CNT adsorbent. This finding is in agreement with the nature of this adsorption being more efficient at low pH, as discussed earlier in section 3.3. Next, we studied the effect of the amount of HNO_3 on the etching process by using 5 different concentrations of the acid in the range of 0.1–2.0 M. It turned out that

as the HNO_3 concentration increases, the removal efficiency increases as well. Finally, the number of regeneration cycles was investigated as illustrated in Figure 10. In this figure, the first cycle (no. 1) resembles the removal efficiency before washing. The successive cycles were obtained by washing the residue with 0.1 M HNO_3 . It is clear from Figure 10 that the removal efficiency of cycle 2 exceeds the original experiment. Finally, Figure 10 illustrates that the regeneration of KP is successful up to 5 cycles.

Adsorption mechanism using DFT calculations

The adsorption mechanism of KP on both Fe_3O_4 and CNT was explored at the PBE-D/DZP level as detailed in the experimental section. The adsorption on Fe_3O_4 was done by testing different adsorption sites around the slab. The most stable geometry was found to be the one parallel to the 110 (xy) direction, as illustrated in Figure 11. The adsorption energy (E_{ad}) was calculated to be -50.0 kJ/mol, indicating favorable adsorption as defined by eq. 8. The optimized geometry in Figure 11 also shows strong Van der Waals forces between the acidic sites in KP, the O–H group in particular, and the dangling oxygen atoms in Fe_3O_4 . The distance between the acidic proton in KP and the closest O atom in Fe_3O_4 is 1.28 Å, which lies in the range of hydrogen bond.

Figure 12 shows the results of the adsorption study of KP inside and outside the carbon nanotube model. The average C–C bond distance between the KP molecule and the adjacent carbon on the CNT was found to be 3.7–4.2 Å, in the inside geometry (Figure 12-left). In the outside geometry (Figure 12-right), the bond distance was averaged between 3.0–3.4 Å. This indicates that the KP molecule is closer to the CNT when it is

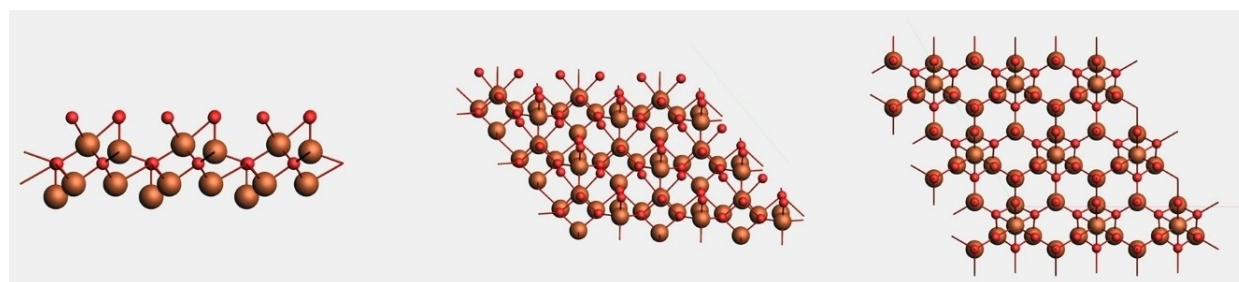


Figure 13. Different views of the (111) Fe_3O_4 slab model used in this work, optimized at PBE-D/DZP level of theory.

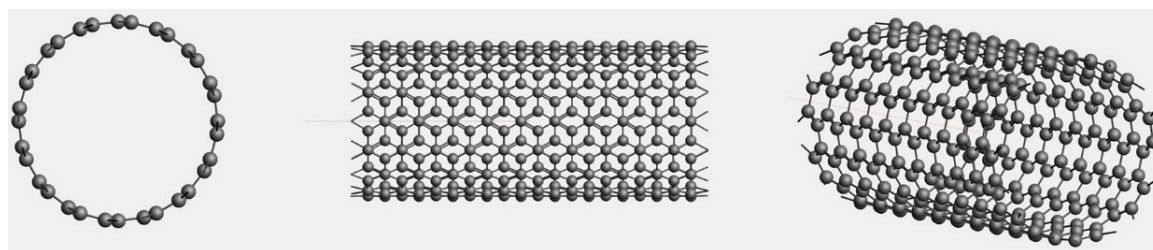


Figure 14. Different views of the (8, 8) carbon nanotube slab model used in this work, optimized at PBE-D/DZP level of theory.

situated outside the surface. However, It was found that E_{ad} is equal to -38.8 and -168.5 kJ/mol, for the outside and inside geometries, respectively. Clearly, the placement of KP inside the CNT is much more favorable than being on the surface. When the molecule is encircled by the CNT ring, rather than being outside, the strong electrostatic interactions between the drug's molecule and the π -system of the CNT can explain this discrepancy. The results of our calculations therefore suggests that adsorption of KP is mostly favorable inside the CNT. Also, the adsorption on the CNT surface is equally favorable to the one of Fe_3O_4 , due to the close values of E_{ad} . The computational results also reinforce the dual adsorption theory that has been discussed in the previous sections.

Conclusion

The removal of the anti-inflammatory drug ketoprofen (KP) was examined by a new magnetic adsorbent. The nano adsorbent was sanitized in situ by impregnating MWCNT into Fe_3O_4 (Fe/CNT). SEM, XRD, FTIR and EDX analysis showed a highly crystalline and pure material. The nano adsorbent was also easy to separate by a magnet. The adsorption of KP on the Fe/CNT surface was both fast and efficient. The maximum adsorption capacity was determined to be 39.2 mg/g which reflects the high efficiency of the new nano adsorbent. The adsorption was highly pH dependent, and the best removal efficiency was obtained at $pH \approx 4$. This dependency was discussed in terms of the point of zero charge of the adsorbent and the pK_a of the drug. It was evident that electrostatic attractions between the protonated form of the drug and the positively charged Fe/CNT surface were strong at low pH, leading to high adsorption efficiency. On the other hand, the repulsion forces between the anionic form of KP and the negatively charged surface have led to weaker adsorption at higher pH. The adsorption isotherms were following a sigmoidal behavior and they were best fitted to the corresponding-states equation (CSE), The physical meaning of such behavior is based on the dual adsorption theory, under which the adsorption process switches from monolayer to multilayer coverage. This is because the adsorbent used in this study is a composite of iron oxides and the highly efficient MWCNT. The adsorption kinetics was also investigated by following the value of q_e as a function of time, and the adsorption was found to follow second-order kinetics. This meant that the adsorbent is abundant with active sites, in support of the sigmoidal model.

The effect of temperature on adsorption was studied and the values of ΔH° and ΔS° were determined to be -38.0 kJ/mol and -158.9 JK $^{-1}$ mol $^{-1}$, respectively. A regeneration study was made by etching the adsorbent with NaOH and HNO $_3$. It was found that the latter is more efficient in regenerating the adsorbent so it could be recycled and used for further cycles. This is in concert with the adsorption being more favorable in acidic medium. The regeneration was shown to be active up to 5 cycles. Periodic DFT calculations revealed that the adsorption of KP is much more favorable when the drug's molecule is placed within the CNT cavity rather than being on the CNT

surface. Also, the calculations suggested that the adsorption is equally favorable on the CNT and the Fe_3O_4 surfaces.

Experimental Section

Materials

Ketoprofen (2-[3-Benzoylphenyl]propionic acid, C $_{16}$ H $_{14}$ O $_3$, 254.3 g/mol) was purchased from Alfa Aesar, Massachusetts, USA. Iron (II) sulfate (FeSO $_4$, 99%) and ammonia solution (26% NH $_3$) were purchased from Riedel-de Haen, Germany. Iron (III) sulphate hydrate (Fe $_2$ (SO $_4$) $_3$ ·xH $_2$ O, 400 g/mol, 99%) was obtained from Research Lab Fine Chem, India. Multi-walled carbon nanotubes (MWCNT, outer diameter = 5–15 nm, length = 10–30 μ m) were purchased from Nanjing XFNano Material Tech Co. Ltd. China. For preparing the buffer solutions, nitric acid (HNO $_3$, 69%) and acetic acid (glacial, 99.55%) were obtained from Loba Chemie Pvt. Ltd, India. Sodium acetate (CH $_3$ COONa, 99%) was obtained from Research Lab Fine Chem, India. Ammonium chloride (99.5%) was purchased from Sigma-Aldrich Chemie GmbH, Taufkirchen, Germany. The neodymium magnets (model DIYMAG F60103 20P) used in this work were purchased from Amazon.com, Inc. Washington, USA.

Instruments

For the adsorption experiments, samples were weighed using an analytical balance (Adam Equipment, UK). Aqueous samples were shaken using an orbital and linear shaker (model Sk-O180-PRO, Biobase Ltd. India).

The shaking power was 15 W and the shaking speed is shaking speed = 350 rpm, unless it is mentioned otherwise. The pH was adjusted using a portable pH Meter (mode PH400S, Apera Instruments, Ohio, USA) and mixed using an ultrasonic cleaner (model 2800, Branson Ultrasonics Corporation, Connecticut, USA). For the temperature study, a 28.0-L analog shaking water bath (model NE5-28, Nickel-Electro Ltd. UK) was used. The concentrations of KP were determined by a UV-Vis Spectrophotometer (model UV-2700i, Shimadzu. Maryland, USA). The scanning electron microscope (SEM) images for the nano adsorbent were collected using a field emission instrument (Nova Nano SEM 450) operating at 5 kV and equipped with an energy dispersive X-ray analyzer (EDX, Bruker). The crystal structure of the nanocomposite was analyzed using an X-ray diffractometer (MiniFlex 2, Applied Rigaku Technologies, Inc., Texas, USA) equipped with nickel filtered CuK α radiation ($k = 0.1564$ nm) operated at 30 kV and 15 mA. The XRD scans were done in the range of 10–30 $^\circ$ for 2 hr at a scan speed of 1.8 $^\circ$ /min. The Fourier transform infrared (FTIR) spectra were recorded using a PerkinElmer spectrometer (model Spectrum BX II). The samples were dried overnight at 80 $^\circ$ C then pressed into pellets with KBr prior to analysis.

Synthesis of Fe $_3$ O $_4$ /MWCNT

The Fe $_3$ O $_4$ /MWCNT nanocomposite, referred by Fe/CNT, was prepared by mixing 24.055 g of Fe $_2$ (SO $_4$) $_3$ ·xH $_2$ O and 4.512 g of FeSO $_4$ in 75 mL of deionized water. The reaction was started immediately to avoid oxidation of the iron (II) ions. 1.5 g of MWCNT was added to the mixture under continuous stirring. This provided 1.4% CNT to the total iron precursors by mass. 50 mL of concentrated ammonia solution (26% NH $_3$) were added dropwise to the mixture over 5 min. The stirring was continued for 3 hours at 60 $^\circ$ C, and the

mixture pH was kept above 10 by adding ammonia as needed. It is critical to keep a basic solution in order to obtain the blackish Fe_3O_4 and avoid further oxidation to Fe_2O_3 (brown). The mixture was then allowed to cool to room temperature and then washed with deionized water and ethanol to obtain a clear solution. The magnetic nanoparticles were then separated using a powerful neodymium magnet and dried overnight at 80°C .

Adsorption experiments

To assess the adsorption capacity of the Fe/CNT adsorbent, the effect of the adsorbent dosage was first studied in batch mode. In a typical experiment, a specific mass in the range of 1–200 mg of the freshly synthesized Fe/CNT was weighed and added to 50-mL Erlenmeyer flasks. Then, 25 mL of 100 mg/L of KP ($M = 254.3$ g/mol) were added to the flask and the solution was covered and shaken for a specific time at room temperature. The KP-contaminated NPs were separated from the solution by using a neodymium magnet and the supernatant was transferred to a new container. No filtration was performed to avoid any side adsorption by filter papers. The concentration of KP after adsorption was determined by reading its absorbance spectra at $\lambda_{\text{max}} = 260$ nm.

For the pH study, different buffer solutions were prepared at different pH values using reagent grade deionized water as previously reported.^[39] Standard solutions of KP were prepared in each buffer solution. The final pH of the standard solutions was adjusted using diluted NaOH or HCl at ambient temperature. As for determining the point of zero charge (PZC) of the adsorbent, 10 different solutions with the same ionic strength were prepared at different pH values in the range of 1–12. For each solution, 40.0 mL of NaNO_3 (0.1 M) were added to an Erlenmeyer flask and the pH was adjusted using dilute HNO_3 (0.1 M) or NaOH (0.1 M). The exact pH was measured and considered the initial pH. Then, 20 mg of the freshly prepared Fe/CNT adsorbent were added to each flask and the mixtures were shaken at speed of 350 rpm for 20 h. Once equilibrium is established, the pH was measured again and considered as pH final. A plot of initial pH vs. final pH was constructed and the PZS was considered to be the cross point between the two.^[75–76]

For the temperature study, the adsorption experiments were performed at isothermal conditions. This was achieved by thermostating all stock solutions at the desired temperature in a water bath. The adsorption experiments and the UV-Vis spectra were all done at the same temperature.

In order to measure the reusability of the Fe/CNT nanoadsorbent, the NPs were separated by a magnet and washed with 0.1 M HNO_3 . The supernatant was transferred to a new container and its UV-Vis spectrum was recorded. The process was repeated for several cycles until the adsorption efficiency came to an end.

Quantum theoretical calculations

The periodic density functional calculations involved in this work were performed using the BAND engine in Amsterdam Modeling Suite (AMS) 2022.^[77–78] The magnetite (Fe_3O_4) crystal structure used in the calculations was obtained from the reported *cif* file.^[79] The structure belongs to the cubic $F\bar{4}3m$ space group with reported parameters of $a=b=c=8.3941$ Å. The most stable form of magnetite is the one lying on the (111) surface.^[80–82] so a (111) slab was sliced, and a supercell of Fe_3O_4 was constructed as shown in Figure 13.

As for the CNT model, a (8, 8) nanotube with a length of ten rings was constructed as shown in Figure 14. The Perdew-Burke-Ernzerhof (PBE) exchange correlation functional augmented with Grimme's dispersion (PBE-D).^[83–84] was used to optimize the structures along with the double- ζ basis set (DZP). The final single point energies were computed using the triple- ζ basis set (TZP). This level of theory was selected based on its good performance in similar studies.^[80–82,85] Structure optimization was done using the scalar relativistic effect with the ZORA approach,^[86–87] and the smallest frozen core approximation.^[87] All calculations were done with an energy cut-off of 0.0001 Ha and a gradient convergence of 0.005 Ha/Å.

The adsorption of KP on the Fe_3O_4 slab was done by placing the pre-optimized KP molecule next to the slab surface and allowing the system to optimize at PBE-D/DZP level of theory. During optimization, the metal surface slab was fixed in position. The adsorption energy (E_{ad}) was calculated as:^[88]

$$E_{\text{ad}} = E_{\text{adsorbate/surface}} - (E_{\text{surface}} + E_{\text{adsorbate}}) \quad (8)$$

where $E_{\text{adsorbate/surface}}$ is the total energy of the optimized slab/KP system, E_{surface} is the total energy of the optimized Fe_3O_4 slab, and $E_{\text{adsorbate}}$ is the energy of optimized KP molecule. The format of eq. 8 implies that a negative E_{ad} value corresponds to stronger adsorption.^[88–89] Similarly, adsorption of KP on CNT was done either by placing the drug's molecule on or inside the nanotube. More details on such calculations can be found in our recent published work.^[89]

Supporting Information Summary

The Supporting Information section include information on the method validation, the method's reproducibility and sensitivity, and the method detection limit (MDL). The UV-Vis spectra of the blanks and the KP's solution. EDX spectra of pure MWCNT, and Fe_3O_4 /MWCNT nanocomposite. Adsorption isotherms of KP into Fe/CNT with fitting curves according to different adsorption models at different pH values. Nonlinear fitting for the adsorption of KP on Fe/CNT.

Acknowledgements

The authors are grateful to the Department of Chemistry, the Faculty of Science at An-Najah National University, and the Departments of Chemistry at Qatar University for supporting this research. This research is partially funded by the student grant QUST-1-CAS-2021-2. The authors are also thankful to the staff at the Central Lab Unit (CLU) at Qatar University for helping in performing the SEM/EDX analysis.

Conflict of Interest

The authors declare no conflict of interest.

Data Availability Statement

The data that support the findings of this study are available in the supplementary material of this article.

Keywords: adsorption · carbon nanotubes · DFT · iron oxide · mechanism · pharmaceutical

- [1] F. A. Kibuye, H. E. Gall, K. R. Elkin, B. Ayers, T. L. Veith, M. Miller, S. Jacob, K. R. Hayden, J. E. Watson, H. A. Elliott, *Sci. Total Environ.* **2019**, *654*, 197–208.
- [2] A. Kot-Wasik, A. Jakimska, M. Śliwka-Kaszyńska, *Environ. Monit. Assess.* **2016**, *188*, 661.
- [3] Y. Luo, W. Guo, H. H. Ngo, L. D. Nghiem, F. I. Hai, J. Zhang, S. Liang, X. C. Wang, *Sci. Total Environ.* **2014**, *473–474*, 619–641.
- [4] C. F. Couto, L. C. Lange, M. C. S. Amaral, *J. Water Proc. Eng.* **2019**, *32*, 100927.
- [5] M. Qiu, L. Liu, Q. Ling, Y. Cai, S. Yu, S. Wang, D. Fu, B. Hu, X. Wang, *Biochar* **2022**, *4*, 19.
- [6] A. Panagopoulos, K.-J. Haralambous, *J. Environ. Chem. Eng.* **2020**, *8*, 104418.
- [7] Y. Muhammad, W. Lee, *Sci. Total Environ.* **2019**, *681*, 551–563.
- [8] I. Badran, Z. Talie, *Iran. J. Chem. Chem. Eng.* **2020**, -.
- [9] I. Badran, A. D. Manasrah, N. N. Nassar, *RSC Adv.* **2019**, *9*, 13403–13413.
- [10] I. W. Almanassra, V. Kochkodan, G. Ponnusamy, G. McKay, M. Ali Atieh, T. Al-Ansari, *J. Environ. Health* **2020**, *18*, 1375–1390.
- [11] M. Zeng, M. Chen, D. Huang, S. Lei, X. Zhang, L. Wang, Z. Cheng, *Mater. Horiz.* **2021**, *8*, 758–802.
- [12] J. Wang, S. Wang, *J. Environ. Manage.* **2016**, *182*, 620–640.
- [13] A. J. Ebele, M. Abou-Elwafa Abdallah, S. Harrad, *Emerging Contam.* **2017**, *3*, 1–16.
- [14] I. Badran, A. Hassan, A. D. Manasrah, N. N. Nassar, *J. Therm. Anal. Calorim.* **2019**, *138*, 433–441.
- [15] M. S. Diniz, R. Salgado, V. J. Pereira, G. Carvalho, A. Oehmen, M. A. M. Reis, J. P. Noronha, *Sci. Total Environ.* **2015**, *505*, 282–289.
- [16] N. S. Riyaz, I. Badran, *J. Therm. Anal. Calorim.* **2022**, *147*, 10755–10765.
- [17] M. Zeng, P. Wang, J. Luo, B. Peng, B. Ding, L. Zhang, L. Wang, D. Huang, I. Echols, E. Abo Deeb, E. Bordovsky, C.-H. Choi, C. Ybanez, P. Meras, E. Situ, M. S. Mannan, Z. Cheng, *ACS Appl. Mater. Interfaces* **2018**, *10*, 22793–22800.
- [18] J. Zhang, L. Feng, Y. Jian, G. Luo, M. Wang, B. Hu, T. Liu, J. Li, Y. Yuan, N. Wang, *Chem. Eng. J.* **2022**, *429*, 132265.
- [19] N. Ouasfi, M. Zbair, S. Bouzikri, Z. Anfar, M. Bensitel, H. Ait Ahsaine, E. Sabbar, L. Khamliche, *RSC Adv.* **2019**, *9*, 9792–9808.
- [20] Z. A. Alothman, A. Y. Badjah, O. M. Alduhaish, K. Rathinam, S. Panglisch, I. Ali, *J. Mol. Liq.* **2021**, *323*, 115075.
- [21] E. Prichard, E. F. Granek, *Environ. Sci. Pollut. Res. Int.* **2016**, *23*, 22365–22384.
- [22] A. F. M. Streit, G. C. Collazzo, S. P. Druzian, R. S. Verdi, E. L. Foletto, L. F. S. Oliveira, G. L. Dotto, *Chemosphere* **2021**, *262*, 128322.
- [23] K. Styszko, J. Szczyrowski, N. Czuma, D. Makowska, M. Kistler, Ł. Uruski, *Int. J. Environ. Sci. Technol.* **2018**, *15*, 493–506.
- [24] G. D. Alkmin, A. M. V. M. Soares, C. Barata, B. Nunes, *Environ. Pollut.* **2020**, *265*, 114993.
- [25] D. Smiljanić, B. de Gennaro, F. Izzo, A. Langella, A. Daković, C. Germinario, G. E. Rottinghaus, M. Spasojević, M. Mercurio, *Microporous Mesoporous Mater.* **2020**, *298*, 110057.
- [26] H. Abu Hasan, S. R. Sheikh Abdullah, A. W. N. Al-Attabi, D. A. H. Nash, N. Anuar, N. Abd. Rahman, H. Sulistiyuning Titah, *Sep. Purif. Technol.* **2016**, *157*, 215–221.
- [27] J. Fischer, C. R. Ganellin, *Chemistry International–Newsmagazine for IUPAC* **2010**, *32*, 12–15.
- [28] I. M. Minisy, N. A. Salahuddin, M. M. Ayad, *Polym. Bull.* **2021**, *78*, 5609–5622.
- [29] L. E. Mofokeng, L. Hlekelele, Z. N. Tetana, J. Moma, V. P. Chauke, *ChemistrySelect* **2022**, *7*, e202101847.
- [30] (FDA) The U. S. Food and Drug Administration, FDA, USA, **2020**.
- [31] V. Naidoo, K. Wolter, D. Cromarty, M. Diekmann, N. Duncan, A. A. Meharg, M. A. Taggart, L. Venter, R. Cuthbert, *Biology letters* **2010**, *6*, 339–341.
- [32] A. C. Fröhlich, E. L. Foletto, G. L. Dotto, *J. Cleaner Prod.* **2019**, *229*, 828–837.
- [33] A. E. B. Kermia, D. Fouial-Djebbar, M. Trari, *C. R. Chim.* **2016**, *19*, 963–970.
- [34] S. Dahane, M. D. Gil García, M. J. Martínez Bueno, A. Uclés Moreno, M. Martínez Galera, A. Derdour, *J. Chromatogr. A* **2013**, *1297*, 17–28.
- [35] J. L. Santos, I. Aparicio, E. Alonso, M. Callejón, *Anal. Chim. Acta* **2005**, *550*, 116–122.
- [36] M. Rabiet, A. Togola, F. Brissaud, J.-L. Seidel, H. Budzinski, F. Elbaz-Poulichet, *Environ. Sci. Technol.* **2006**, *40*, 5282–5288.
- [37] O. Y. Bakather, A. Kayvani Fard, Ihsanullah, M. Khraisheh, M. S. Nasser, M. A. Atieh, *Bioinorg. Chem. Appl.* **2017**, *2017*, 4323619.
- [38] N. N. Nassar, A. Hassan, L. Carbognani, F. Lopez-Linares, P. Pereira-Almao, *Fuel* **2012**, *95*, 257–262.
- [39] I. Badran, R. Khalaf, *Sep. Sci. Technol.* **2019**, *55*, 2433–2448.
- [40] D. Ewis, A. Benamor, M. M. Ba-Abbad, M. Nasser, M. El-Naas, H. Qiblawey, *J. Water Proc. Eng.* **2020**, *38*, 101583.
- [41] K. S. M. Salih, W. R. Thiel, in *Palladium-Catalyzed Coupling Reactions* **2013**, 57–78.
- [42] K. S. M. Salih, P. Mamone, G. Dörr, T. O. Bauer, A. Brodyanski, C. Wagner, M. Kopnarski, R. N. Klupp Taylor, S. Demeshko, F. Meyer, V. Schünemann, S. Ernst, L. J. Gooßen, W. R. Thiel, *Chem. Mater.* **2013**, *25*, 1430–1435.
- [43] I. Badran, O. Qut, A. D. Manasrah, M. Abualhasan, *Environ. Sci. Pollut. Res. Int.* **2020**.
- [44] M. E. A. El-sayed, *Sci. Total Environ.* **2020**, *739*, 139903.
- [45] A. D. Manasrah, I. W. Almanassra, N. N. Marei, U. A. Al-Mubaiyedh, T. Laoui, M. A. Atieh, *RSC Adv.* **2018**, *8*, 1791–1802.
- [46] H. Sadegh, G. A. M. Ali, A. S. H. Makhlof, K. F. Chong, N. S. Alharbi, S. Agarwal, V. K. Gupta, *J. Mol. Liq.* **2018**, *258*, 345–353.
- [47] J. Tang, J. Wang, *ChemistrySelect* **2017**, *2*, 10727–10735.
- [48] C. M. Kerkhoff, K. da Boit Martinello, D. S. Franco, M. S. Netto, J. Georgan, E. L. Foletto, D. G. Piccilli, L. F. Silva, G. L. Dotto, *J. Mol. Liq.* **2021**, *339*, 117184.
- [49] V. Rizzi, J. Gubitosa, P. Fini, R. Romita, S. Nuzzo, P. Cosma, *Materials* **2019**, *12*, 3810.
- [50] L. M. Madikizela, S. S. Zunngu, N. Y. Mlunguza, N. T. Tavengwa, P. S. Mdluli, L. Chimuka, *Water SA* **2018**, *44*, 406–418.
- [51] I. A. Lawal, M. M. Lawal, S. O. Akpotu, M. A. Azeez, P. Ndungu, B. Moodley, *Ecotoxicol. Environ. Saf.* **2018**, *161*, 542–552.
- [52] Y. Wang, L. He, G. Dang, H. Li, X. Li, *J. Colloid Interface Sci.* **2021**, *592*, 51–65.
- [53] P. A. Ajibade, E. C. Nnadozie, *Environ. Chem. Ecotoxicol.* **2022**, *4*, 140–147.
- [54] S. Li, Y. Gong, Y. Yang, C. He, L. Hu, L. Zhu, L. Sun, D. Shu, *Chem. Eng. J.* **2015**, *260*, 231–239.
- [55] S. Kurwadkar, T. V. Hoang, K. Malwade, S. R. Kanel, W. F. Harper, G. Struckhoff, *Nanotechnol. Environ. Eng.* **2019**, *4*, 12.
- [56] D. Bhatia, D. Datta, A. Joshi, S. Gupta, Y. Gote, *J. Mol. Liq.* **2019**, *276*, 163–169.
- [57] V. J. Inglezakis, S. G. Pouloupoulos, H. Kazemian, *Microporous Mesoporous Mater.* **2018**, *272*, 166–176.
- [58] C. Battersack, *Phys. Chem. Chem. Phys.* **2019**, *21*, 5614–5626.
- [59] G. Limousin, J. P. Gaudet, L. Charlet, S. Szenknect, V. Barthès, M. Krimissa, *Appl. Geochem.* **2007**, *22*, 249–275.
- [60] C. J. Radke, J. M. Prausnitz, *Ind. Eng. Chem. Fundam.* **1972**, *11*, 445–451.
- [61] M. Alizadeh Fard, B. Barkdoll, *Int. J. Environ. Sci. Technol.* **2019**, *16*, 1625–1636.
- [62] Y. Liu, Z. Zhao, D. Yuan, Y. Wang, Y. Dai, Y. Zhu, J. W. Chew, *Appl. Surf. Sci.* **2019**, *466*, 893–902.
- [63] L. Ji, L. Zhou, X. Bai, Y. Shao, G. Zhao, Y. Qu, C. Wang, Y. Li, *J. Mater. Chem.* **2012**, *22*, 15853–15862.
- [64] M. Abdel Salam, M. A. Gabal, A. Y. Obaid, *Synth. Met.* **2012**, *161*, 2651–2658.
- [65] K. V. Kumar, *J. Hazard. Mater.* **2006**, *137*, 1538–1544.
- [66] J. Wang, X. Guo, *J. Hazard. Mater.* **2020**, *390*, 122156.
- [67] E. C. Lima, A. Hosseini-Bandegharaei, J. C. Moreno-Piraján, I. Anastopoulos, *J. Mol. Liq.* **2019**, *273*, 425–434.
- [68] P. W. Atkins, J. De Paula, J. Keeler, *Atkins' Physical chemistry*, 11th ed., Oxford University Press, Oxford, United Kingdom ; New York, NY, **2018**.
- [69] Y. Liu, *J. Chem. Eng. Data* **2009**, *54*, 1981–1985.
- [70] S. Wang, C. W. Ng, W. Wang, Q. Li, L. Li, *J. Chem. Eng. Data* **2012**, *57*, 1563–1569.
- [71] Y. Lu, Y. Li, Y. Gao, B. Ai, W. Gao, G. Peng, *Water Sci. Technol.* **2020**, *81*, 1461–1470.
- [72] A. C. Fröhlich, G. S. dos Reis, F. A. Pavan, É. C. Lima, E. L. Foletto, G. L. Dotto, *Environ. Sci. Pollut. Res. Int.* **2018**, *25*, 24713–24725.
- [73] I. A. Lawal, M. M. Lawal, S. O. Akpotu, M. A. Azeez, P. Ndungu, B. Moodley, *Ecotoxicol. Environ. Saf.* **2018**, *161*, 542–552.

- [74] L. Sellaoui, L. F. O. Silva, M. Badawi, J. Ali, N. Favarin, G. L. Dotto, A. Erto, Z. Chen, *J. Mol. Liq.* **2021**, *333*, 115906.
- [75] S. K. Bajpai, A. Jain, *Water* **2012**, *4*, 52–71.
- [76] E. N. Bakatula, D. Richard, C. M. Neculita, G. J. Zagury, *Environ. Sci. Pollut. Res. Int.* **2018**, *25*, 7823–7833.
- [77] G. te Velde, E. J. Baerends, *Phys. Rev. B* **1991**, *44*, 7888–7903.
- [78] E. S. Kadantsev, R. Klooster, P. L. De Boeij, T. Ziegler, *Mol. Phys.* **2010**, *105*, 2583–2596.
- [79] M. E. Fleet, *J. Solid State Chem.* **1986**, *62*, 75–82.
- [80] X. Yu, S.-G. Wang, Y.-W. Li, J. Wang, H. Jiao, *J. Phys. Chem. C* **2012**, *116*, 10632–10638.
- [81] M. Busch, V. Mehar, L. R. Merte, M. Shipilin, E. Lundgren, J. F. Weaver, H. Grönbeck, *Chem. Phys. Lett.* **2018**, *693*, 84–87.
- [82] J. Ahdjoudj, C. Martinsky, C. Minot, M. A. Van Hove, G. A. Somorjai, *Surf. Sci.* **1999**, *443*, 133–153.
- [83] S. Grimme, S. Ehrlich, L. Goerigk, *J. Comput. Chem.* **2011**, *32*, 1456–1465.
- [84] J. P. Perdew, Y. Wang, *Phys. Rev. B* **1992**, *45*, 13244.
- [85] X. Li, J. Paier, *J. Phys. Chem. C* **2016**, *120*, 1056–1065.
- [86] P. Philippen, E. Van Lenthe, J. Snijders, E. Baerends, *Phys. Rev. B* **1997**, *56*, 13556.
- [87] V. Pershina, M. Iliaš, *Inorg. Chem.* **2019**, *58*, 9866–9873.
- [88] Z. Yan, J. Fan, Z. Zuo, Z. Li, J. Zhang, *Appl. Surf. Sci.* **2014**, *288*, 690–694.
- [89] I. Badran, N. Sahar Riyaz, A. M. Shraim, N. N. Nassar, *Comput. Theor. Chem.* **2022**, *1211*, 113689.

Submitted: August 1, 2022

Accepted: September 23, 2022